JOC The Journal of Organic Chemistry

Article

pubs.acs.org/joc

Extended π-Conjugated Molecules Derived from Naphthalene Diimides toward Organic Emissive and Semiconducting Materials

Yonghai Li, Guanxin Zhang,* Ge Yang, Yunlong Guo, Chong'an Di, Xin Chen, Zitong Liu, Huiying Liu, Zhenzhen Xu, Wei Xu, Hongbing Fu, and Deqing Zhang*

Beijing National Laboratory for Molecular Sciences, Organic Solids Laboratory and Photochemistry Laboratory, Institute of Chemistry, Chinese Academy of Sciences, Beijing 100190, China

Supporting Information

ABSTRACT: In this paper, a new synthetic way to modify naphthalene diimide (NDI) at "shoulder" positions is reported. The key step of the transformation is the intramolecular cyclization involving ethynyl and imidecarbonyl groups. The structure of the intermediate pyrylium cation was confirmed by X-ray crystal structural analysis. New conjugated molecules **1a**−**g** were successfully synthesized in acceptable yields. Their absorption and fluorescence spectra were measured. Among them **1c**−**f** are strongly emissive in solutions. Furthermore, **1b**−**f** are also fluorescent in their solid states; in particular, **1b** exhibits a typical aggregation-induced enhanced emission feature. Yellow-emissive microfibrils of **1d** show potential optical waveguide behavior. HOMO/LUMO energies of **1a**−**f** were determined based on their cyclic voltammograms. The results also reveal that HOMO/LUMO energies of these new conjugated molecules are influenced by the two flanking moieties. Notably, the thin film of **1c** that is emissive shows *p*-type semiconducting behavior with hole mobility up to 0.0063 $cm^2 V^{-1} s^{-1}$ based on the transfer and output characteristics of the OFET (organic field effect transistor).

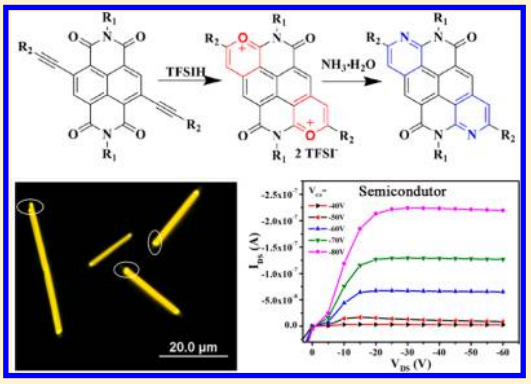

INTRODUCTION

It is well-known that development of new π-conjugated molecules is crucial for optoelectronic materials including light-emitting materials, organic semiconductors, and photovoltaic materials.[1−11] This is mainly owing to the electronic structure of π-systems, which can lead to extensive delocalization of electrons throughout the molecules. In principle, HOMO/LUMO energies and their intermolecular interactions (thus self-assembly structures) of π-conjugated molecules can be tuned by modifying their chemical structures. In this manner, emissive and electronic properties of π-conjugated molecules in the solid states are critically determined by their chemical structures. More and more results reveal that extended π-conjugated molecules are promising for optoelectronic materials of high performances. Accordingly, extended π-conjugated molecules have received increasing attention in recent years.[12−15]

1,4,5,8-Naphthalenediimide (NDI) and its derivatives have been intensively investigated for organic optoelectronic materials.[16−18] Organic semiconductors and photovoltaic materials have been constructed on the basis of NDI framework.[19,20] In order to enhance the performance of NDI-based materials, various chemical modifications of the NDI framework were reported. As depicted in Scheme 1, these can be mainly classified as follows: (i) connection of electron-withdrawing or -donating moieties to the NDI core via single bonds;[21−25] (ii) fusion of additional rings to NDI at core positions;[26−30] (iii) chemical modification of the imide groups of NDI and formation of additional rings at "head" positions;[31−35] (iv) transformation of the imide groups of NDI into additional rings at "shoulder" positions.[36,37]

Scheme 1. Illustration of Chemical Modification Manners of NDI to Extended Conjugated Molecules

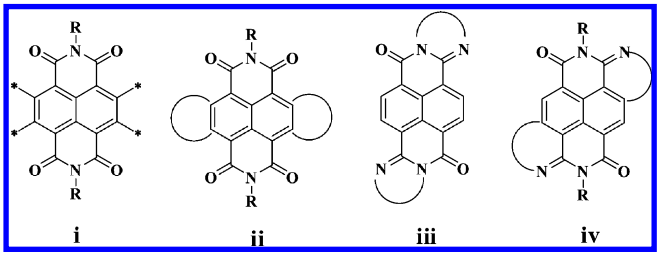

A number of NDI-derived conjugated molecules were prepared via manner i. For instance, incorporation of electron-withdrawing −CN groups at the core positions of NDI led to air-stable *n*-type semiconductors.[21,22] Facchetti et al. reported the alternating NDI-bithiophene polymer, and the resulting OFETs exhibited electron mobilities up to 0.85 $cm^2 V^{-1} s^{-1}$ (*n*-type) under ambient conditions.[23−25] Chemical modification of NDI via manner ii also led to various π-

Received: December 14, 2012
Published: March 5, 2013

   dx.doi.org/10.1021/jo302677k | J. Org. Chem. 2013, 78, 2926−2934

Scheme 2. Chemical Structures and Synthetic Approaches for Compounds 1a−g, 2a−g, and 3a−g[a]

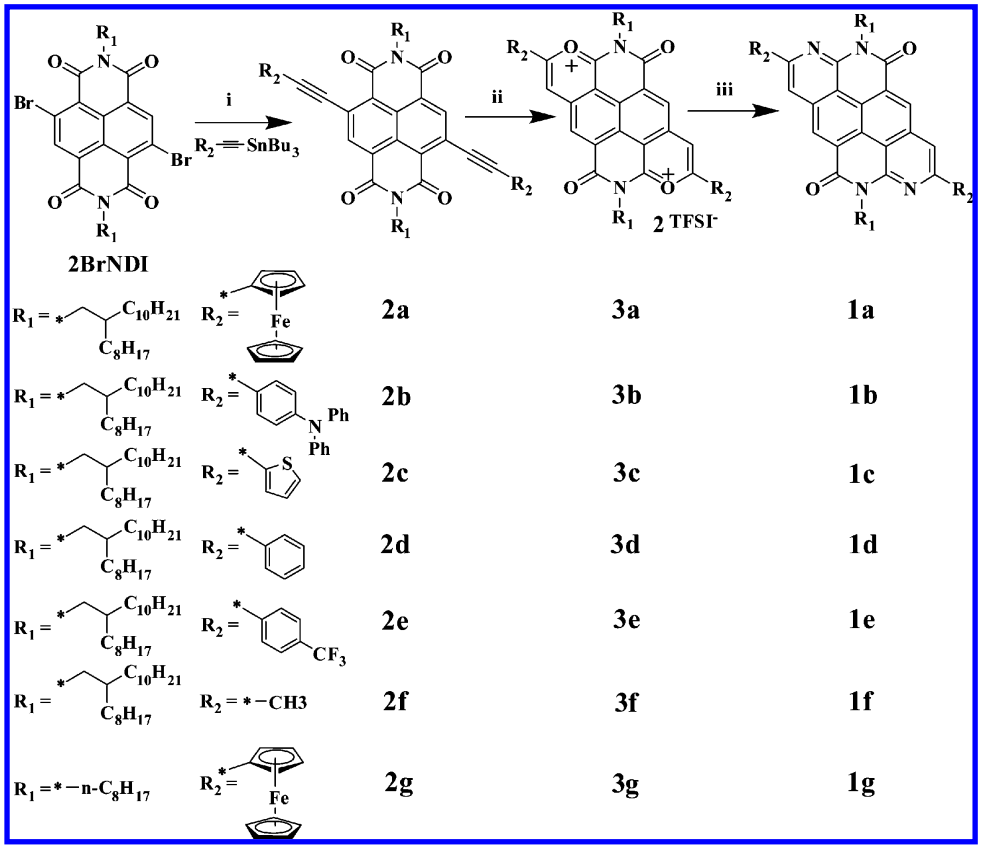

[a]Reagents and conditions: (i) respective tin reagents, $Pd(PPh_3)_4$, toluene, reflux, 2.5 h; yields: for **2a**, 81%; for **2b**, 84%; for **2c**, 86%; for **2d**, 89%; for **2e**, 85%; for **2f**, 76%; for **2g**, 83%; (ii) TFSIH (bis(trifluoromethane)sulfonamide), CH_2Cl_2, N_2, for **2a−d** and **2g**, rt 0.5−6.0 h; for **2e**,**f**, reflux, 48 h; (iii) $NH_3·H_2O$, CH_3OH, reflux, 1.0 h; yields based on **2a−g**, respectively: for **1a**, 47%; for **1b**, 42%; for **1c**, 60%; for **1d**, 52%; for **1e**, 46%; for **1f**, 59%; for **1g**, 58%.

conjugated molecules for organic semiconductors of high mobilities. Gao et al. reported core-expanded NDI derivatives containing 2-(1,3-dithiol-2-ylidene)malonitrile groups (electron-withdrawing), and the resulting OFETs exhibit electron mobilities up to 1.2 $cm^2\ V^{-1}\ s^{-1}$ in air (*n*-type).[26−28] Würthner et al. disclosed *p*-type and ambipolar semiconductors based on core-expanded NDI.[29] Some of us have very recently described NDI derivatives entailing electron-donating tetrathiafulvalene or 1,3-dithole-2-thione (-one) moieties, and they behave as either *n*-type or *p*-type or ambipolar materials depending on the substitution groups.[30]

Chemical transformations of the imide groups of NDI were also explored to generate new conjugated molecules (via manners iii and iv). Perinone derivatives as industrially important pigments were synthesized via manners iii many decades ago.[31] However, in recent years, this type of modified NDI framework is getting more attention from other areas. For example, Jenekhe and co-workers introduced them into ladder-polymers which exhibit *n*-type semiconducting properties.[32,33] Langhals et al. reported naphthalene iminoimides by either condensation of NDI with ethylenediamine or simultaneous condensation of naphthalene dianhydride, a primary amine, and ethylenediamine.[34] Marks et al. have recently disclosed a family of naphthaleneamidinemonoimide-fused oligothiophenes that exhibit *n*-type or ambipolar semiconducting behaviors.[35] However, fusion of rings to NDI at the "shoulder" positions was seldom reported. Marder and co-workers have just recently described the transformation of NDI into the 2,6-diacyl derivatives, which can react with hydrazine to afford 2,6-diacylnaphthalene-1,8:4,5-bis(dicarboximides).[36] This modified-NDI framework has been also incorporated into ladder-polymers by Luscombe et al., and these electronic polymers exhibit electron mobilities as high as 0.0026 $cm^2\ V^{-1}\ s^{-1}$ (*n*-type).[37]

In this paper, we report a new synthetic approach to modify NDI at "shoulder" positions to yield new extended conjugated molecules **1a−g** (Scheme 2). Spectroscopic and electrochemical studies were performed to determine their HOMO/LUMO levels. Most of these new conjugated molecules were found to be emissive both in solutions and solid states. Moreover, thin-film OFET (organic field-effect transistor) of **1c** was successfully fabricated, which behaved as a *p*-type semiconductor with hole mobility up to 0.0063 $cm^2\ V^{-1}\ s^{-1}$. These studies clearly manifest that these new NDI-derived conjugated molecules are interesting building blocks to construct new optoelectronic materials.

RESULTS AND DISCUSSION

Synthesis. The synthesis of **1a−f** started from the respective NDI compounds **2a−f** with substituted acetylene moieties which were prepared by Stille coupling of the respective tin reagents and **2BrNDI** (dibromonaphthalene diimide, *N*-$C_{20}H_{41}$).[38] Compounds **2a−f** were allowed to react with TFSIH [bis(trifluoromethane)sulfonamide] under nitrogen atmosphere to afford colored solids after removal of

dx.doi.org/10.1021/jo302677k | J. Org. Chem. 2013, 78, 2926−2934

solvents. As to be discussed below, these colored solids were the products from intramolecular cyclization involving ethynyl and imidecarbonyl groups in CH_2Cl_2. These colored solids were dissolved in dry methanol and treated with $NH_3 \cdot H_2O$ under reflux. After separation with column chromatography, **1a−f** were obtained in acceptable yields. Their structures were characterized by NMR and MS data, and their purities were confirmed by elemental analysis.

It is interesting to note that the transformation of **2a−c** with electron-donating groups at the end of ethynyl groups into the colored solids can be completed after stirring at room temperature for less than 1 h. The transformation of **2d** can also easily proceed after stirring at room temperature for about 6.0 h. However, the transformation of **2e** and **2f** required heating the CH_2Cl_2 solutions to reflux for about 48 h. These are indeed in agreement with the formation of intermediate compounds **3a−f** since the electron-donating groups will stabilize the pyrylium cations, whereas electron-accepting groups would not be favorable for the formation of the respective pyrylium cations. Crystals of good quality were not obtained for the colored solids **3a−f**. Instead, the analogous compound **1g** with short alkyl chains ($-n$-C_8H_{17}) at the *N*-positions was synthesized by following the same procedures as for **1a**. The crystal structure of **3g** was successfully determined. As depicted in Figure 1, the formation of the pyrylium cation

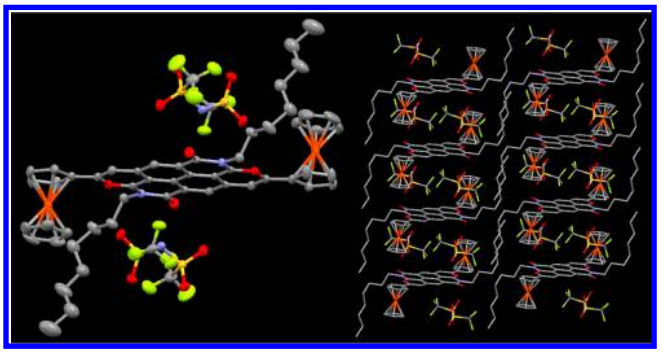

Figure 1. Crystal structure of **3g** and the intermolecular arrangements in the crystal.

3g was clearly confirmed. The central part of **3g** flanked by two ferrocene moieties was completely planar. Two Cp (cyclopentadienyl) rings in two flanking ferrocene moieties are almost coplanar with the central core. The bond lengths and angles of **3g** are all in the normal region (see the Supporting Information). To conclude briefly, the crystal structure of **3g** provides solid evidence for the formation of the pyrylium cation through the intramolecular cyclization involving the ethynyl and imidecarbonyl groups.

Although Nishihara and co-workers reported protonation-induced cyclization of 1-arylethynylanthraquinones and relevant molecules,[39−41] the intramolecular reaction between ethynyl and imidecarbonyl groups to form pyrylium cation in the presence of acid was not reported before, to the best of our knowledge. This new reaction will not only provide a new approach to modify NDI at "shoulder" positions but also enlarge the scope of this type of cyclization reaction reported initially by Nishihara.[41] This versatile reaction allows the formation of two pyridine rings and simultaneous introduction of different functional groups, which can be either electron-withdrawing or donating, to generate new extended conjugated molecules.

Spectroscopic Studies. The solutions of **1a−g** are colorful, ranging from red to yellow. The absorption spectra of **1a−g**[42] were measured (see Figure S1, Supporting Information), and the respective low-energy absorption maxima and the coefficients are shown in Table 1. Compound **1f** with two methyl groups shows the absorption maximum at 466 nm. In comparison, the absorptions of **1b−d** are red-shifted. For **1a** with two electron-donating ferrocene moieties the absorption is extended to 620 nm. These results reveal that absorption spectra of **1a−d** are influenced by the flanking groups. This can be understood as follows: (1) the flanking moieties in **1a−d** are electron-donating, whereas the central cores are electron-accepting; (2) thus, intramolecular interactions between the respective electron-donating and -accepting moieties in **1a−d** are anticipated; (3) absorption spectra of **1a−d** are expected to be influenced by such intramolecular interactions.[43] The introduction of electron-withdrawing (*p*-trifluoromethyl)phenyl moieties in **1e** will weaken the intramolecular electron donor−acceptor interactions, and as a result the absorptions of **1e** are slightly hypsochromically shifted compared to those of **1c** and **1d** as depicted in Figure S1 (Supporting Information).

Both **1a** and **1g** are almost nonfluorescent in solutions. Figure 2a shows the fluorescence spectra of **1b−f** including

Table 1. Absorption and Fluorescence Data of 1a−f

		fluorescence							
	absorption[a]	solution fluorescence			solid-state fluorescence				
compd	λ_{max}[b] (nm) (ε/$M^{-1}cm^{-1}$)	λ_{max}[c] (nm)	Φ[d]	τ (ns)	λ_{max} (nm)	Φ[e]	τ_1 (ns)	τ_2 (ns)	$<\tau>$[f] (ns)
1a	453 (22400)								
1b	515 (16000)	637	0.06		605	0.24	15.26		15.26
1c	504 (25500)	521	0.40	3.84	614	0.05	1.04	4.47	3.44
1d	480 (28500)	490	>0.99	7.04	545	0.30	1.44	8.15	5.47
1e	472 (27700)	482	>0.99	4.26	538	0.10	0.88	3.15	1.95
1f	466 (35600)	476	>0.99	10.32	543	0.08	7.96	0.94	4.02

[a]The absorption spectra were measured with the respective CH_2Cl_2 solutions; the concentration of each solution was 1.0×10^{-5} M. [b]Lowest energy absorption maxima. [c]The fluorescence spectra were measured with the respective CH_2Cl_2 solutions, and the concentration of each solution was 1.0×10^{-5} M; the excitation wavelengths were 515 nm for **1b**, 475 nm for **1c**, 455 nm for **1d**, 440 nm for **1e**, and 430 nm for **1f**, respectively. [d]The solution quantum yields were measured using rhodamine 101 (Φ = 100% in ethanol) as standard. [e]The quantum yields in the solid states were measured using the absolute integrating sphere method. [f]An apparent decay time constant $<\tau>$ (average fluorescence lifetime) was determined by using the relation $<\tau = \sum_{i=1}^{n} a_i \times \tau_i / \sum_{i=1}^{n} a_i>$ (n = 1−2), where τ_i and a_i, respectively, represent the individual exponential decay time constant and the corresponding preexponential factor.[55]

dx.doi.org/10.1021/jo302677k | J. Org. Chem. 2013, 78, 2926−2934

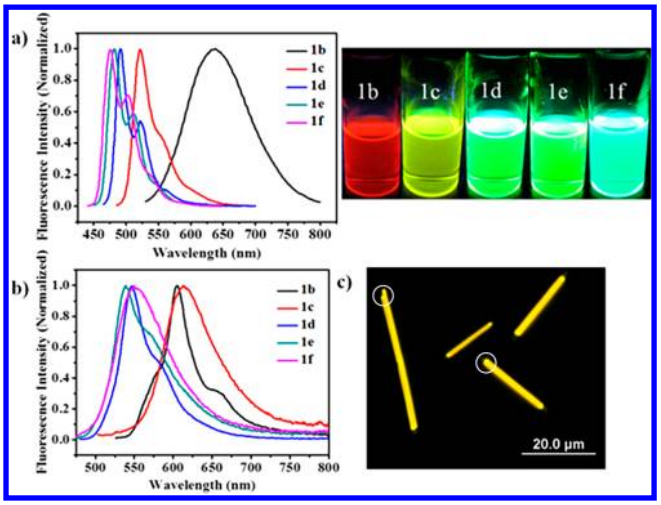

Figure 2. (a) (Left) Solution fluorescence spectra of **1b**–**f** in CH_2Cl_2; the concentration of each solution was 1.0×10^{-5} M. (Right) Corresponding solution photos of **1b**–**f** (1.0×10^{-3} M in CH_2Cl_2) under UV light (365 nm) irradiation; (b) solid-state fluorescence spectra of **1b**–**f** in the form of powders; (c) photoluminescence (PL) images of microfibrils of **1d**.

photos of their solutions under UV light, and Table 1 summarizes their emission maxima and quantum yields. Obviously, the emissive properties of **1b**–**f** are influenced by the features of the flanking groups. The emission maxima are red-shifted in the following order: **1f** < **1e** < **1d** < **1c** < **1b**. The solutions of **1d**–**f** show bright yellow-green fluorescence, and their emission quantum efficiencies reach that of Rhodamine 101. The solution of **1b** emits red light with low quantum efficiency, whereas the solution of **1c** is yellow-emissive with relatively high quantum efficiency. The fluorescence lifetimes of **1c**–**f** are in the nanosecond region, being in agreement with their high quantum efficiencies. These results reveal that the emission properties of **1a**–**g** can be tuned by the flanking groups: (1) when the flanking groups such as ferrocene in **1a** and **1g** and triphenylamine in **1b** are electron-donating the fluorescence will be largely quenched due to the photoinduced electron transfer;[44] (2) the incorporation of electron-donating groups will also red-shift the emission.

The solid-state fluorescence spectra were also measured (see Figure 2b), and the respective emission quantum yields and fluorescence lifetimes including average fluorescence lifetimes are listed in Table 1. Again, **1a** and **1g** are not emissive in the solid state either.[45] Other compounds are fluorescent in their solid states. Among these compounds, **1b** and **1d** are strongly emissive with relatively high emission quantum yields in the solid states. This is consistent with the observation that **1b** and **1d** show longer average fluorescence lifetimes than those of **1c**, **1e**, and **1f**. In comparison with the fluorescence behaviors of **1c**–**f** in solutions, their emission maxima are red-shifted and emission quantum yields are reduced in their solid states. This may be attributed to the intermolecular π–π interactions in solid states of **1c**–**f** according to previous reports.[46]

Yellow-emissive microfibrils of **1d** were obtained and characterized with photoluminescence microscopy. Notably, the tips of these microfibrils exhibit even brighter yellow-emission as depicted in Figure 2c. Therefore, microfibrils of **1d** are potentially useful for optical waveguides.[47]

However, compared to those of **1b** in solution, the emission maximum of **1b** in the solid state is hypsochromically shifted and the emission quantum yield is enhanced (see Table 1). As shown in Figure 3, the CH_2Cl_2 solution of **1b** is just weakly

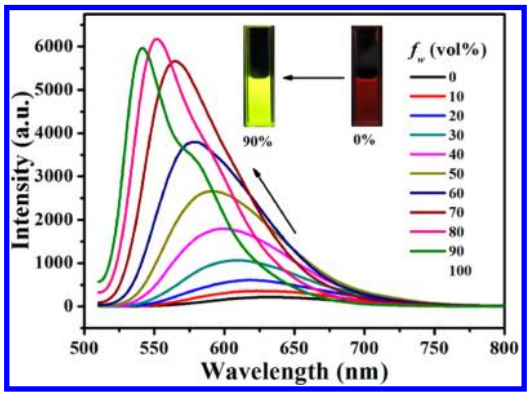

Figure 3. Fluorescence spectra of **1b** (1.0×10^{-5} M) in the mixture of CH_2Cl_2 and *n*-hexane with different fractions of *n*-hexane (f_w); the excitation wavelength was 500 nm. When only *n*-hexane was used as the solvent, it was found that a small amount of **1b** precipitated out and as a result the fluorescence intensity was slightly reduced.

emissive; but after the addition of *n*-hexane to induce the aggregation of **1b** the fluorescence spectrum is gradually hypsochromically shifted and fluorescence intensity is simultaneously enhanced. For instance, the emission maximum is shifted from 637 to 551 nm and the intensity increases by 46.5-fold when the volume content of *n*-hexane reaches 90%. Such "unexpected" fluorescent behavior of **1b** may be ascribed to the free-rotation of phenyl fragments within triphenylamine moieties which will lead to weak fluorescence of **1b** in solution;[48] however, these rotations can be inhibited in the solid state (after aggregation), resulting in fluorescence enhancement according to previous reports.[49−53] The blue-shift of the emission maximum in the solid state (after aggregation) is probably due to the fat that **1b** adopts a more twisting conformation in the solid state; as a result, the intramolecular electron donor–acceptor interactions are weakened and the emission is hypsochromically shifted.[54]

Electrochemical and Theoretical Studies. Cyclic voltammgrams of **1a**–**f** were measured, and their redox potentials are shown in Table 2. As shown in Figure S9 (Supporting Information), **1a** and **1b** each possess one quasi-reversible oxidation wave due to ferrocence and triphenylamine moieties, respectively;[56] both of them also exhibit one quasi-reversible reduction wave and one irreversible reduction wave. In comparison, **1c**–**f** each exhibit an irreversible oxidation wave at potentials higher than 1.30 V (vs Ag/AgCl), but they each also possess one quasi-reversible reduction wave and one irreversible reduction wave. On the basis of the respective onset oxidation and reduction potentials, HOMO and LUMO energies of **1a**–**f** were estimated with the following equations: HOMO = $-(E_{onset}^{ox1} + 4.41)$ eV, LUMO = $-(E_{onset}^{red1} + 4.41)$ eV.[57,58] As listed in Table 2, HOMO energies of **1a** and **1b** are −4.91 and −5.30 eV, respectively, which lie higher than those of **1c**–**f**. This is likely owing to the presence of two electron-donating groups in **1a** and **1b**. LUMO energies of **1c** and **1e** lie lower than those of **1a**, **1b**, **1d**, and **1f**. The incorporation of electron-withdrawing groups (*p*-trifluoromethylphenyl) in **1e** is beneficial for lowering its LUMO energy. Theoretical calculation (see below) indicates that the two thiophene rings in **1c** are almost coplanar with the central core. Such coplanar conformation favors electron delocalization, and accordingly it

dx.doi.org/10.1021/jo302677k | J. Org. Chem. 2013, 78, 2926−2934

Table 2. Redox Potentials and Experimental/Calculated HOMO/LUMO Energies of 1a–f[a]

	experimental data							DFT calculations	
compd	E_p^{red1} (V)	E_p^{ox1} (V)	E_{onset}^{red1} (V)	E_{onset}^{ox1} (V)	HOMO (eV)	LUMO (eV)	E_g^{cv} (eV)	HOMO (eV)	LUMO (eV)
1a	−1.37	0.74	−1.20	0.50	−4.91	−3.21	1.70		
1b	−1.27	1.09	−1.16	0.89	−5.30	−3.25	2.05		
1c	−1.32	1.53	−1.09	1.35	−5.76	−3.32	2.44	−5.54	−2.67
1d	−1.36	1.74	−1.14	1.52	−5.93	−3.27	2.66	−5.69	−2.65
1e	−1.23	1.79	−1.00	1.65	−6.06	−3.41	2.65	−6.03	−2.93
1f	−1.32	1.66	−1.18	1.52	−5.93	−3.23	2.70	−5.80	−2.59

[a]The redox potentials were presented in reference to Ag/AgCl, which was calibrated.

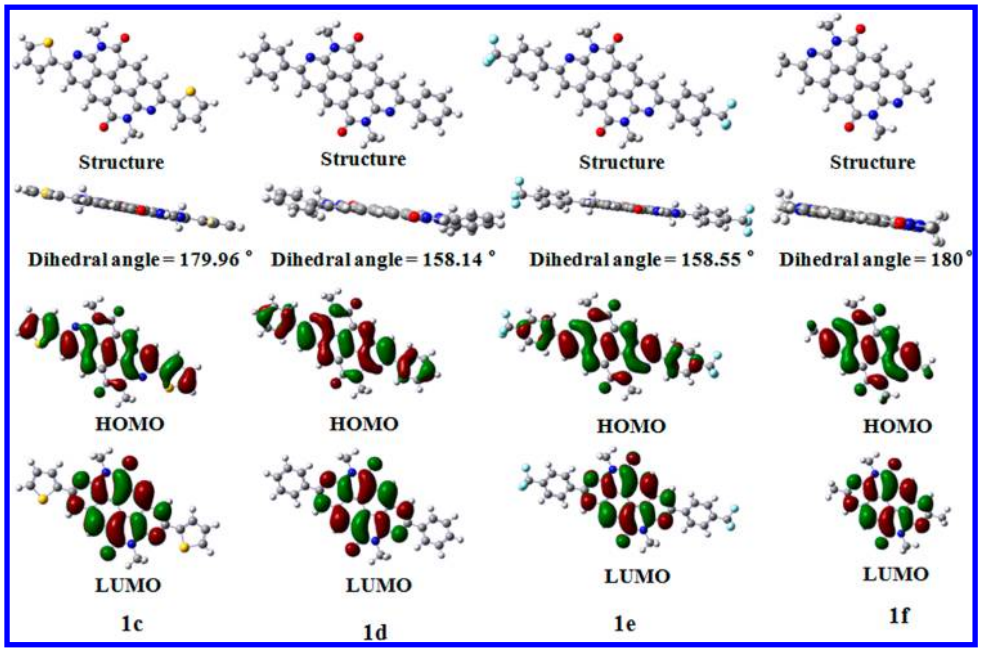

Figure 4. Calculated structures, dihedral angles, and HOMO/LUMO orbitals of **1c–f** based on DFT calculations; the alkyl chains were replaced by methyl groups in the calculations.

is understandable that the HOMO and LOMO energies of **1c** were slightly enhanced and lowered, respectively, in comparison with those of **1d**. Therefore, for this type of modified-NDI conjugated molecules their HOMO/LUMO energies can be tuned by varying the respective two flanking moieties.

The structures of **1c–f** were investigated with theoretical calculations based on density functional theory (DFT).[59] It is expected that the alkyl chains at the *N*,*N*′-positions of the new π-expanded NDI core should not have a significant influence on their electronic structures. Thus, the alkyl chains were replaced by methyl groups for the DFT calculations. As depicted in Figure 4, the central core of **1c–f** is completely planar. The two thiophene rings in **1c** are almost coplanar with the central core, but the respective two flanking moieties in **1d** and **1e** form dihedral angles of ca. 158° with the central core. HOMO orbitals of **1c–f** are delocalized on both the central core and the respective flanking groups, whereas LUMO orbitals are mostly localized on the central core (see Figure 4). The calculated HOMO/LUMO energies of **1c–f** (see Table 2) are different from those based on their cyclic voltammograms,[60] but the results do indicate that HOMO/LUMO energies of these new extended conjugated molecules are affected by the respective two flanking moieties.

Organic Field-Effect Transistor with Thin Film of 1c. Theoretical calculations reveal that **1c** prefers to adopt a planar conformation; thus, intermolecular π–π interactions are expected for the thin film of **1c**. For this reason, OFET with thin a film of **1c** was fabricated to demonstrate the potential application of these new conjugated molecules as organic semiconductors. The fabrication details of OFET are discussed in the Experimental Section. Figure 5 shows the transfer and output characteristics of the bottom-gate bottom-contact OFET with thin-film of **1c**. Obviously, I_{DS} increases by applying the negative V_{GS}. Thus, it can be concluded that the thin film of **1c** behaves as a *p*-type semiconductor. As depicted in Table S1 (Supporting Information), hole mobilities of OFETs with thin films of **1c** increase after annealing the thin films of **1c** at 80 and 100 °C. For instance, the OFETs with thin films of **1c** exhibit hole mobility up to 0.0063 $cm^2\ V^{-1}\ s^{-1}$ (0.0054 $cm^2\ V^{-1}\ s^{-1}$ on average) with on/off ratios up to 10^6 after annealing at 100 °C. But, the performance of OFETs of **1c** becomes poor after further increasing the annealing temperature to 120 °C (see Table S1, Supporting Information). Further optimization of OFET fabrication is underway to improve the OFET performance.

XRD studies reveal that the crystallinity of the thin film of **1c** is improved upon annealing. The as-prepared thin-film exhibited no diffraction peaks, and weak diffraction peaks at 2θ = 6.1° and 2θ = 12.2° appeared after annealing at 80 °C. However, intensities of diffraction peaks at 2θ = 6.1° and 2θ = 12.2° increased, and new peaks at 2θ = 9.1, 21.4, and 23.8° emerged after annealing at 100 °C (see Figure S11, Supporting

dx.doi.org/10.1021/jo302677k | J. Org. Chem. 2013, 78, 2926–2934

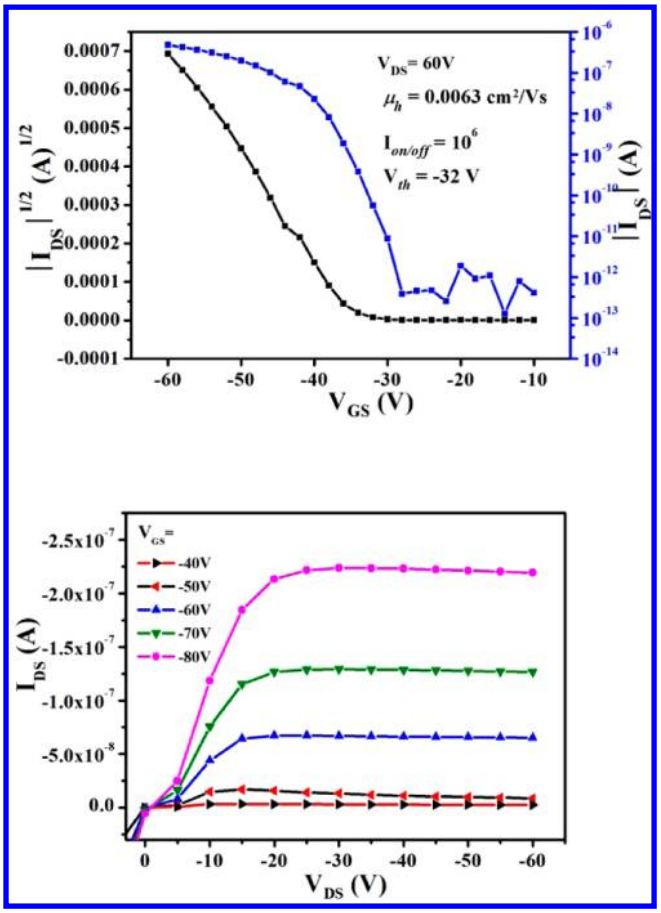

Figure 5. Transfer characteristics (a) and output characteristics (b) for OFET of **1c** after annealing at 100 °C; the channel width (W) and length (L) were 1440 and 50 μm, respectively.[64].

Information). The crystallinity enhancement observed for the thin film of **1c** agrees well with the observation that hole mobility increases after annealing. AFM images were also measured for the thin ilm of **1c** after annealing at different temperatures (see Figure S11, Supporting Information). Thin-film morphology is obviously altered after annealing the thin-film of **1c**. Relatively large domains which are interconnected are formed after annealing at 100 °C.[61] According to previous reports,[62,63] such thin-film morphology is beneficial for enhancing carrier mobility.

CONCLUSION

In conclusion, we disclose a new synthetic approach to transform NDI into extended conjugated molecules. The key step of the transformation is the intramolecular cyclization involving ethynyl and imidecarbonyl groups. New conjugated molecules **1a–f** were successfully synthesized in acceptable yields. The structure of the intermediate pyrylium cation was confirmed by X-ray crystal structural analysis. Except for **1a**, compounds **1b–f** are emissive in solutions and their emission characters can be tuned by varying the respective two flanking moieties. Furthermore, **1b–f** are also fluorescent in their solid states; in particular, **1b** exhibits aggregation-induced enhanced emission. Yellow-emissive microfibrils of **1d** show potential optical waveguide behavior. The results also reveal that HOMO/LUMO energies of **1a–f**, which were determined on the basis of their cyclic voltammograms, are influenced by the two flanking moieties. Notably, the thin film of **1c** that is emissive behaves as a *p*-type semiconducting behavior with hole mobility up to 0.0063 $cm^2\ V^{-1}\ s^{-1}$.

It is expected that this new NDI-derived conjugated framework is promising for constructing new optoelectronic materials since different functionalities can be easily introduced to this framework. Alternatively, compounds **1c** and **1d** can be transformed into the corresponding **1c**-2Br and **1d**-2Br (see Chart 1), which can be utilized as new building blocks to prepare new conjugated D–A molecules and polymers toward electronic materials of high performance. Therefore, this new conjugated framework that is easily accessible from NDI deserves further studies.

Chart 1

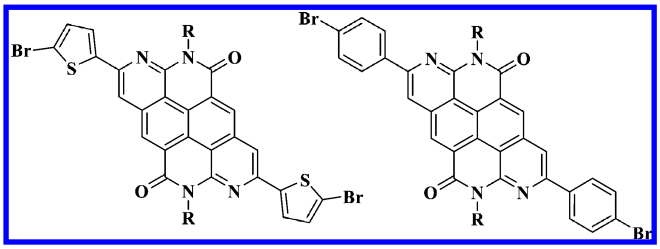

EXPERIMENTAL SECTION

2BrNDI (*N*-*n*-C_8H_{17}, *N*-$C_{20}H_{41}$) were synthesized according to the reported procedures.[65] The corresponding tin reagents were synthesized according to the reported procedures and used directly without further purification.[66]

Synthesis of 2a. A solution of 2BrNDI (*N*-$C_{20}H_{41}$) (108 mg, 0.11 mmol), tributyl(2-ferrocenylethynyl)stannane (165 mg, 0.33 mmol), and a catalytic amount of $Pd(PPh_3)_4$ in toluene (30 mL) was refluxed for 2.5 h under nitrogen atmosphere. After the reaction, the solvent was evaporated under vacuum and the residue was subjected to silica gel column chromatography with petroleum ether (60–90 °C)/CH_2Cl_2 (v/v, 1/1) as eluent. Compound **2a** was obtained as a dark green solid (110 mg, 0.088 mmol) in 81% yield: mp 149.3–150.1 °C; ^{1}H NMR (400 MHz, $CDCl_3$) δ 8.80 (s, 2H), 4.72 (br, 4H), 4.42 (br, 4H), 4.33 (s, 10H), 4.18 (d, J = 6.6 Hz, 4H), 2.04 (br, 2H), 1.35–1.23 (m, 64H), 0.86 (m, 12H); ^{13}C NMR (100 MHz, $CDCl_3$) δ 162.8, 162.1, 137.4, 127.5, 126.4, 124.8, 105.0, 87.3, 72.6, 70.7, 70.4, 64.1, 45.0, 36.7, 32.1, 31.9, 30.2, 29.8, 29.5, 26.6, 22.8, 14.3; MS (MALDI-TOF) m/z 1243.0 (M^+). Anal. Calcd for $C_{78}H_{102}Fe_2N_2O_4$: C, 75.35; H, 8.27; N, 2.25. Found: C, 75.38; H, 8.29; N, 2.35.

Synthesis of 2b. Compound **2b** was synthesized as for compound **2a** and obtained as a blue solid in 84% yield: mp 170.8–172.1 °C; ^{1}H NMR (400 MHz, CD_2Cl_2): δ 8.64 (s, 2H), 7.46 (d, J = 8.3 Hz, 4H), 7.25 (m, 8H), 7.06 (m, 12H), 6.94 (d, J = 8.3 Hz, 4H), 4.03 (d, J = 6.7 Hz, 4H), 1.92 (br, 2H), 1.34–1.12 (m, 64H), 0.78–0.73 (m, 12H); ^{13}C NMR (100 MHz, $CDCl_3$) δ 162.7, 162.0, 149.5, 146.9, 137.2, 134.0, 129.7, 127.2, 126.5, 125.7, 124.9, 124.5, 124.3, 121.4, 114.8, 104.4, 90.3, 44.9, 36.5, 32.0, 31.7, 30.2, 29.8, 29.5, 26.5, 22.8, 14.3; MS (MALDI-TOF) m/z 1361.7 (M^+). Anal. Calcd for $C_{94}H_{112}N_4O_4$: C, 82.90; H, 8.29; N, 4.11. Found: C, 82.80; H, 8.24; N, 4.13.

Synthesis of 2c. Compound **2c** was synthesized as for compound **2a** and obtained as a red solid in 86% yield: mp 142.8–143.4 °C; ^{1}H NMR (400 MHz, $CDCl_3$) δ 8.79 (s, 2H), 7.56 (d, J = 1.9 Hz, 2H), 7.49 (d, J = 4.5 Hz, 2H), 7.12 (br, 2H), 4.15 (d, J = 6.7 Hz, 4H), 2.03 (br, 2H), 1.43–1.22 (m, 64H), 0.85–0.89 (m, 12H); ^{13}C NMR (100 MHz, $CDCl_3$) δ 162.5, 161.9, 136.9, 134.9, 130.6, 127.8, 126.8, 126.6, 125.2, 124.8, 122.7, 96.6, 94.3, 45.0, 36.6, 32.1, 31.8, 30.2, 29.8, 29.5, 26.5, 22.8, 14.3; MS (MALDI-TOF) m/z 1038.9 (M^+). Anal. Calcd for $C_{66}H_{90}N_2O_4S_2$: C, 76.25; H, 8.73; N, 2.69. Found: C, 75.93; H, 8.69; N, 2.76.

Synthesis of 2d. Compound **2d** was synthesized as for compound **2a** and obtained as an orange solid in 89% yield: mp 120.1–120.6 °C;

dx.doi.org/10.1021/jo302677k | J. Org. Chem. 2013, 78, 2926–2934

^{1}H NMR (400 MHz, $CDCl_3$) δ 8.84 (s, 2H), 7.75 (br, 4H), 7.45 (br, 6H), 4.16 (d, J = 6.7 Hz, 4H), 2.04 (br, 2H), 1.44−1.22 (m, 64H), 0.86−0.85 (m, 12H); ^{13}C NMR (100 MHz, $CDCl_3$) δ 162.5, 161.9, 137.4, 132.8, 130.0, 128.7, 127.3, 126.6, 125.5, 125.2, 122.7, 103.0, 89.7, 45.0, 36.6, 32.1, 31.8, 30.2, 29.8, 29.5, 26.5, 22.8, 14.3; MS (MALDI-TOF) m/z 1027.0 (M^+). Anal. Calcd for $C_{70}H_{94}N_2O_4$: C, 81.82; H, 9.22; N, 2.73. Found: C, 81.83; H, 9.11; N, 2.56.

Synthesis of 2e. Compound **2e** was synthesized similarly as for compound **2a** and obtained as an orange-yellow solid in 85% yield: mp 119.6−120.5 °C; ^{1}H NMR (400 MHz, $CDCl_3$) δ 8.77 (s, 2H), 7.83 (d, J = 8.0 Hz, 4H), 7.68 (d, J = 8.1 Hz, 4H), 4.13 (d, J = 7.1 Hz, 4H), 2.00 (br, 2H), 1.42−1.21 (m, 64H), 0.87−0.82 (m 12H); ^{13}C NMR (150 MHz, $CDCl_3$) δ 162.1, 161.5, 137.1, 132.9, 126.7, 126.3, 125.9, 125.6, 125.3, 124.8, 100.8, 91.2, 45.1, 36.6, 32.1, 31.8, 30.2, 29.8, 29.8, 29.5, 26.5, 22.8, 14.2; MS (MALDI-TOF) m/z 1162.7 (M^+). Anal. Calcd for $C_{72}H_{92}F_6N_2O_4$: C, 74.32; H, 7.97; N, 2.41. Found: C, 73.99; H, 8.07; N, 2.49.

Synthesis of 2f. Compound **2f** was synthesized as for compound **2a** and obtained as a yellow solid in 76% yield: mp 117.8−118.2 °C. ^{1}H NMR (400 MHz, $CDCl_3$) δ 8.68 (s, 2H), 4.11 (d, J = 7.4 Hz, 4H), 2.32 (s, 6H), 2.00 (br, 2H), 1.39−1.22 (m, 64H), 0.93−0.87 (m, 12H); ^{13}C NMR (100 MHz, $CDCl_3$) δ 162.4, 162.1, 138.0, 128.2, 126.2, 125.5, 125.0, 101.6, 80.0, 45.1, 36.5, 32.0, 31.7, 30.2, 29.8, 29.5, 26.5, 22.8, 14.2; MS (MALDI-TOF) m/z 902.8 (M^+). Anal. Calcd for $C_{60}H_{90}N_2O_4$: C, 79.77; H, 10.04; N, 3.10. Found: C, 79.69; H, 10.24; N, 3.15.

Synthesis of 2g. Compound **2g** was synthesized as for **2a** and obtained as a deep green solid in 71% yield: mp 260.0 °C dec; ^{1}H NMR (400 MHz, $CDCl_3$) δ 8.79 (s, 2H), 4.74 (br, 4H), 4.43 (br, 4H), 4.33 (s, 10H), 4.22 (br, 4H), 1.78 (br, 4H), 1.45−1.29 (m, 20H), 0.88 (br, 6H); ^{13}C NMR (100 MHz, $CDCl_3$) δ 162.4, 161.8, 137.4, 127.4, 126.4, 124.8, 124.7, 105.2, 87.4, 72.7, 70.7, 70.5, 64.1, 41.1, 32.0, 29.5, 29.4, 27.3, 22.8, 14.3; MS (MALDI-TOF) m/z 906.7 (M^+). Anal. Calcd for $C_{54}H_{54}Fe_2N_2O_4$: C, 71.53; H, 6.00; N, 3.09. Found: C, 71.20; H, 6.13; N, 3.14.

Synthesis of 3a−d. TFSIH (39 mg, 0.14 mmol) was added to a solution of **2a** (70 mg, 0.056 mmol) in CH_2Cl_2 (5.0 mL) under nitrogen atmosphere. The solution was stirred for 30 min at room temperature. The solvent was removed under reduced pressure to give **3a** as a purple solid. Compound **3a** was used for next step without further purification. Compounds **3b−d** were synthesized similarly, and they all were used for the next step without further purification.

Synthesis of 3e,f. TFSIH (280 mg, 1.0 mmol) was added to a solution of **2e** (233 mg, 0.20 mmol) in CH_2Cl_2 (15 mL) under nitrogen atmosphere. The solution was refluxed for 24 h. The solvent was removed under reduced pressure to give **3e** as a red solid. Compound **3e** was used for the next step without further purification. Compound **3f** was synthesized similarly as for compound **3e** and used for the next step without further purification.

Synthesis of 3g. Compound **3g** was synthesized similarly as for compound **3a**. However, after the reaction, deep purple crystals were filtered and washed with *n*-hexane to give **3g** in 90% yield: mp 240.0 °C dec; ^{1}H NMR (400 MHz, CD_3CN): δ 9.11 (s, 2H), 8.07 (s, 2H), 5.32 (br, 4H), 5.11 (br, 4H), 4.61 (br, 4H), 4.42 (s, 10H), 1.66 (br, 4H), 1.51−1.35 (m, 20H), 0.91 (br, 6H). Anal. Calcd for $C_{58}H_{56}F_{12}Fe_2N_4O_{12}S_4$: C, 47.42; H, 3.84; N, 3.81. Found: C, 47.13; H, 3.88; N, 3.94.

Synthesis of 1a. To a dry CH_3OH solution (15 mL) of compound **3a** (obtained without further purification, 0.056 mmol) was added $NH_3{\cdot}H_2O$ (0.25 mL, 6.5 mmol). The color immediately changed from deep purple to red, and the solution was refluxed for 1.0 h. Then, the mixture was diluted with water (30 mL) and extracted with CH_2Cl_2 (3 × 20 mL). The organic layer was dried with $MgSO_4$ and concentrated by rotary evaporation. The crude was purified by silica gel column chromatograph with petroleum ether (60−90 °C)/CH_2Cl_2 (v/v, 2/1) as eluent to give **1a** as a red solid (33.5 mg) in 47% yield: mp 178.0 °C dec; ^{1}H NMR (400 MHz, $CDCl_3$) δ 8.96 (s, 2H), 7.77 (s, 2H), 5.14 (br, 4H), 4.63 (d, J = 6.8 Hz, 4H), 4.53 (br, 4H), 4.03 (s, 10H), 2.33 (br, 2H), 1.47−1.19 (m, 64H), 0.86−0.78 (m, 12H); ^{13}C NMR (100 MHz, $CDCl_3$) δ 162.7, 155.2, 149.2, 134.9, 128.0, 125.7, 121.7, 110.9, 109.0, 84.1, 70.6, 70.0, 68.0, 46.2, 36.7, 32.0, 30.3, 29.8, 29.5, 29.4, 27.1, 22.8, 14.25; MS (MALDI-TOF) m/z 1240.9 (M^+). Anal. Calcd for $C_{78}H_{104}Fe_2N_4O_2$: C, 75.47; H, 8.44; N, 4.51. Found: C, 75.61; H, 8.58; N, 4.52.

Synthesis of 1b. Compound **1b** was synthesized similarly and obtained as a red solid (42% yield based on compound **2b**): mp 208.1−209.2 °C; ^{1}H NMR (400 MHz, CD_2Cl_2) δ 8.76 (s, 2H), 8.03 (d, J = 8.2 Hz, 4H), 7.95 (s, 2H), 7.26−7.22 (m, 8H), 7.12−7.07 (m, 12H), 7.04−7.00 (m, 4H), 4.41 (d, J = 6.4 Hz, 4H), 2.09 (br, 2H), 1.24−1.01 (m, 64H), 0.75−0.68 (m, 12H); ^{13}C NMR (100 MHz, $CDCl_3$) δ 162.5, 152.1, 149.3, 147.5, 135.3, 132.0, 129.6, 128.3, 125.6, 125.3, 123.8, 122.6, 121.5, 111.0, 109.2, 46.0, 36.7, 32.0, 31.9, 30.2, 29.8, 29.7, 29.5, 29.4, 26.9, 22.8, 22.8, 14.2; MS (MALDI-TOF) m/z 1359.4 (M^+). Anal. Calcd for $C_{94}H_{114}N_6O_2$: C, 83.02; H, 8.45; N, 6.18. Found: C, 82.94; H, 8.51; N, 6.25.

Synthesis of 1c. Compound **1c** was synthesized similarly and obtained as a orange solid (60% yield based on compound **2c**): mp 202.1−203.3 °C; ^{1}H NMR (400 MHz, $CDCl_3$) δ 8.82 (s, 2H), 7.92 (s, 2H), 7.79 (br, 2H), 7.47 (br, 2H), 7.20 (br, 2H), 4.48 (d, J = 5.2 Hz, 4H), 2.16 (br, 2H), 1.36−1.15 (m, 64H), 0.84−0.81 (m, 12H); ^{13}C NMR (100 MHz, $CDCl_3$) δ 162.0, 149.1, 148.0, 145.0, 135.0, 128.5, 128.4, 125.3, 121.4, 109.9, 109.1, 46.2, 36.5, 32.0, 31.8, 30.3, 29.8, 29.5, 26.7, 22.8, 14.2; MS (MALDI-TOF) m/z 1037.0 (M^+). Anal. Calcd for $C_{66}H_{92}N_4O_2S_2$: C, 76.40; H, 8.94; N, 5.40. Found: C, 76.40; H, 8.99; N, 5.37.

Synthesis of 1d. Compound **1d** was synthesized similarly and obtained as a yellow solid (52% yield based on compound **2d**): mp 142.5−143.4 °C; ^{1}H NMR (400 MHz, $CDCl_3$) δ 8.92 (s, 2H), 8.27 (d, J = 7.3 Hz, 4H), 8.14 (s, 2H), 7.60−7.52 (m, 6H), 4.52 (d, J = 6.6 Hz, 4H), 2.16 (br, 2H), 1.35−1.13 (m, 64H), 0.86−0.79 (m, 12H); ^{13}C NMR (100 MHz, $CDCl_3$) δ 162.3, 152.4, 149.2, 138.7, 135.2, 129.6, 129.1, 128.4, 127.5, 125.5, 121.4, 111.9, 109.3, 46.1, 36.7, 32.0, 30.3, 29.8, 29.5, 26.9, 22.8, 22.8, 14.2; MS (MALDI-TOF) m/z 1025.0 (M^+). Anal. Calcd for $C_{70}H_{96}N_4O_2$: C, 81.98; H, 9.44; N, 5.46. Found: C, 81.88; H, 9.43; N, 5.45.

Synthesis of 1e. Compound **1e** was synthesized similarly and obtained as a yellow solid (46% yield based on compound **2e**): mp 159.5−160.3 °C; ^{1}H NMR (400 MHz, $CDCl_3$) δ 8.98 (s, 2H), 8.32 (d, J = 8.0 Hz, 4H), 8.16 (s, 2H), 7.81 (d, J = 8.1 Hz, 4H), 4.54 (d, J = 7.0 Hz, 4H), 2.16 (br, 2H), 1.23−1.13 (m, 64H), 0.85−0.78 (m, 12H); ^{13}C NMR (150 MHz, $CDCl_3$) δ 162.1, 150.9, 149.6, 141.8, 135.3, 128.6, 127.6, 126.1, 125.2, 123.3, 121.7, 112.6, 109.8, 46.1, 36.7, 32.0, 32.0, 30.3, 29.8, 29.7, 29.4, 26.9, 22.8, 14.2, 14.2; MS (MALDI-TOF) m/z 1160.6 (M^+). Anal. Calcd for $C_{72}H_{94}F_6N_4O_2$: C, 74.45; H, 8.16; N, 4.82. Found: C, 74.51; H, 8.36; N, 4.80.

Synthesis of 1f. Compound **1f** was synthesized similarly and obtained as a yellow solid (59% yield based on compound **2f**): mp 160.1−161.1 °C; ^{1}H NMR (400 MHz, $CDCl_3$) δ 9.09 (s, 2H), 7.71 (s, 2H), 4.69 (d, J = 6.4 Hz, 4H), 2.87 (s, 6H), 2.25 (br, 2H), 1.48−1.19 (m, 64H), 0.87−0.81 (m, 12H); ^{13}C NMR (100 MHz, $CDCl_3$) δ 162.6, 154.1, 149.2, 135.0, 127.5, 125.6, 121.5, 114.6, 108.7, 45.6, 36.6, 32.0, 30.2, 29.8, 29.8, 29.5, 26.7, 25.3, 22.8, 22.8, 14.2; MS (MALDI-TOF) m/z 900.4 (M^+). Anal. Calcd for $C_{60}H_{92}N_4O_2$: C, 79.95; H, 10.29; N, 6.22. Found: C, 79.98; H, 10.29; N, 6.25.

Synthesis of 1g. Compound **1g** was synthesized similarly and obtained as a red solid (58% yield based on compound **2g**): mp 296.0 °C dec; ^{1}H NMR (400 MHz, $CDCl_3$) δ 9.15 (s, 2H), 7.91 (s, 2H), 5.18 (br, 4H), 4.85 (br, 4H), 4.55 (br, 4H), 4.08 (s, 10H), 2.03 (br, 4H), 1.64 (br, 4H), 1.39−1.26 (m, 16H), 0.89 (br, 6H); ^{13}C NMR (75 MHz, 1,2-dichlorobenzene-d_4, 100 °C) δ 161.8, 155.5, 149.3, 135.3, 133.3, 131.0, 122.1, 110.6, 109.4, 84.5, 70.3, 69.8, 68.0, 41.9, 31.9, 29.6, 29.3, 28.4, 27.6, 22.5, 13.8; MS (MALDI-TOF) m/z 904.4 (M^+). Anal. Calcd for $C_{54}H_{56}Fe_2N_4O_2$: C, 71.69; H, 6.24; N, 6.19. Found: C, 71.31; H, 6.12; N, 6.12.

Fabrication of OFETs. Bottom-gate bottom-contact OFETs were fabricated. A heavily doped Si wafer and a layer of dry oxidized SiO_2 (300 nm) were used as a gate electrode and gate dielectric layer, respectively. The drain-source (D-S) gold contacts were fabricated by photolithography. The substrates were cleaned in water, deionized water, ethanol, and rinsed in acetone. Then, the surface was modified

dx.doi.org/10.1021/jo302677k | J. Org. Chem. 2013, 78, 2926−2934

with *n*-octadecyltrimethoxysilane (OTS). After that, the substrates were cleaned in *n*-hexane and $CHCl_3$ and C_2H_5OH. Compound **1c** were dissolved in $CHCl_3$ (about 10 mg/mL) and spin-coated on the substrate at 2000 rpm. The annealing processes were carried out in vacuum condition for 60 min at each temperature.

The field-effect mobility of holes (μ_h) was calculated by fitting a straight line to the plot of the square root of I_{DS} vs V_G (saturation region), according to the expression $I_{DS} = (W/2L)\mu_h C_i(V_G - V_{TH})^2$, where I_{DS} is the drain electrode collected current; L and W are the channel length and width, respectively; μ_h is the mobility of the device; C_i is the capacitance per unit area of the gate dielectric layer; V_G is the gate voltage;and V_{TH} is the threshold voltage.

■ ASSOCIATED CONTENT

Supporting Information

General information, UV−vis absorption, femtosecond transient absorption spectra, fluorescence decay curves, cyclic voltammograms, XRD patterns and AFM images, TGA analysis, X-ray crystallographic data, theoretical calculations data, and ^{1}H NMR and ^{13}C NMR specra. This material is available free of charge via the Internet at http://pubs.acs.org.

■ AUTHOR INFORMATION

Corresponding Author

*E-mail: (G.Z.) gxzhang@iccas.ac.cn, (D.Z.) dqzhang@iccas.ac.cn.

Notes

The authors declare no competing financial interest.

■ ACKNOWLEDGMENTS

The present research was financially supported by NSFC, the State Basic Program, and the Chinese Academy of Sciences.

■ REFERENCES

(1) (a) Li, L.; Gao, P.; Schuermann, K. C.; Ostendorp, S.; Wang, W.; Du, C.; Lei, Y.; Fuchs, H.; Cola, L. D.; Müllen, K.; Chi, L. *J. Am. Chem. Soc.* **2010**, *132*, 8807−8809. (b) Dasgupta, D.; Srinivasan, S.; Rochas, C.; Thierry, A.; Schroeder, A.; Ajayaghosh, A.; Guenet, J. M. *Soft Matter* **2011**, *7*, 2797−2804. (c) Ajayaghosh, A.; J.George, S. *J. Am. Chem. Soc.* **2001**, *123*, 514−517.

(2) (a) Henson, Z. B.; Müllen, K.; Bazan, G. C. *Nature Chem.* **2012**, *4*, 699−704. (b) Chen, L.; Hernandez, Y.; Feng, X.; Müllen, K. *Angew. Chem., Int. Ed.* **2012**, *51*, 7640−7654.

(3) (a) Liu, W. J.; Zhou, Y.; Ma, Y. G.; Cao, Y.; Wang, J.; Pei, J. *Org. Lett.* **2007**, *9*, 4187−4189. (b) Lei, T.; Cao, Y.; Fan, Y.; Liu, C.-J.; Yuan, S.-C.; Pei, J. *J. Am. Chem. Soc.* **2011**, *133*, 6099−6101.

(4) (a) Okamoto, T.; Senatore, M. L.; Ling, M. M.; Mallik, A. B.; Tang, M. L.; Bao, Z. *Adv. Mater.* **2007**, *19*, 3381−3384. (b) Mei, J.; Kim, D. H.; Ayzner, A. L.; Toney, M. F.; Bao, Z. *J. Am. Chem. Soc.* **2011**, *133*, 20130−20133.

(5) (a) Qu, Y.; Hua, J.; Tian, H. *Org. Lett.* **2010**, *12*, 3320−3323. (b) Ning, Z.; Zhang, Q.; Wu, W.; Pei, H.; Liu, B.; Tian, H. *J. Org. Chem.* **2008**, *73*, 3791−3797.

(6) (a) Wang, C.; Dong, H.; Hu, W.; Liu, Y.; Zhu, D. *Chem. Rev.* **2012**, *112*, 2208−2267. (b) Li, R.; Hu, W.; Liu; Zhu, D. *Acc. Chem. Res.* **2010**, *43*, 529−540.

(7) (a) Cao, Y.; Liu, S.; Shen, Q.; Yan, K.; Li, P.; Xu, J.; Yu, D.; Steigerwald, M. L.; Nuckolls, C.; Liu, Z.; Guo, X. *Adv. Funct. Mater.* **2009**, *19*, 2743−2748. (b) Cao, Y.; Steigerwald, M. L.; Nuckolls, C.; Guo, X. *Adv. Mater.* **2010**, *22*, 20−32.

(8) (a) Osaka, I.; Abe, T.; Shinamura, S.; Takimiya, K. *J. Am. Chem. Soc.* **2011**, *133*, 6852−6860. (b) Osaka, I.; Abe, T.; Shinamura, S.; Miyazaki, E.; Takimiya, K. *J. Am. Chem. Soc.* **2010**, *132*, 5000−5001.

(9) (a) Würthner, F. *Angew. Chem., Int. Ed.* **2001**, *40*, 1037−1039. (b) Schmidt, R.; Ling, M. M.; Oh, J. H.; Winkler, M.; Könemann, M.; Bao, Z.; Würthner, F. *Adv. Mater.* **2007**, *19*, 3692−3695.

(10) (a) Liu, Y.; Zhan, X. *Macromol. Chem. Phys.* **2011**, *212*, 428−443. (b) Zhang, Y.; Zou, J.; Cheuh, C.; Yip, H.; Jen, A. K.-Y. *Macromolecules* **2012**, *45*, 5427−5435. (c) Gao, Y.; Yip, H.; Chen, K.; O'Malley, K.; Acton, O.; Sun, Y.; Ting, G.; Chen, H.; Jen, A. K.-Y. *Adv. Mater.* **2011**, *23*, 1903−1908.

(11) Yue, W.; Lv, A.; Gao, J.; Jiang, W.; Hao, L.; Li, C.; Li, Y.; Polander, L. E.; Barlow, S.; Hu, W.; Motta, S.; Negri, F.; Marder, S. R.; Wang, Z. *J. Am. Chem. Soc.* **2012**, *134*, 5770−5773.

(12) Brabec, C. J.; Heeney, M.; McCullochb, I.; Nelsonc, J. *Chem. Soc. Rev.* **2011**, *40*, 1185−1199.

(13) Sergeyev, S.; Pisula, W.; Geerts, Y. H. *Chem. Soc. Rev.* **2007**, *36*, 1902−1929.

(14) Zhou, J.; Wan, X.; Liu, Y.; Long, G.; Wang, F.; Li, Z.; Zuo, Y.; Li, C.; Chen, Y. *Chem. Mater.* **2011**, *23*, 4666−4668.

(15) Chen, H.; Guo, Y.; Yu, G.; Zhao, Y.; Zhang, J.; Gao, D.; Liu, H.; Liu, Y. *Adv. Mater.* **2012**, *24*, 4618−4622.

(16) Bhosale, S. V.; Bhargava, S. K. *Org. Biomol. Chem.* **2012**, *10*, 6455−6468.

(17) Sakai, N.; Mareda, J.; Vautheyb, E.; Matile, S. *Chem. Commun.* **2010**, *46*, 4225−4237.

(18) Würthner, F.; Stolte, M. *Chem. Commun.* **2011**, *47*, 5109−5115.

(19) Zhan, X.; Facchetti, A.; Barlow, S.; Marks, T. J.; Ratner, M. A.; Wasielewski, M. R.; Marder, S. R. *Adv. Mater.* **2011**, *23*, 268−284.

(20) (a) Alam, M. M.; Jenekhe, S. A. *Chem. Mater.* **2004**, *16*, 4647−4656. (b) Ahmed, E.; Ren, G.; Kim, F. S.; Hollenbeck, E. C.; Jenekhe, S. A. *Chem. Mater.* **2011**, *23*, 4563−4577. (c) Fabiano, S.; Chen, Z.; Vahedi, S.; Facchetti, A.; Pignataro, B.; Loi, M. A. *J. Mater. Chem.* **2011**, *21*, 5891−5896. (d) Schubert, M.; Dolfen, D.; Frisch, J.; Roland, S.; Steyrleuthner, R.; Stiller, B.; Chen, Z.; Scherf, U.; Koch, N.; Facchetti, A.; Neher, D. *Adv. Energy Mater.* **2012**, *2*, 369−380.

(21) Chopin, S.; Chaignon, F.; Blart, E.; Odobel, F. *J. Mater. Chem.* **2007**, *17*, 4139−4146.

(22) Chang, J.; Ye, Q.; Huang, K.; Zhang, J.; Chen, Z.; Wu, J.; Chi, C. *Org. Lett.* **2012**, *14*, 2964−2967.

(23) Chen, Z.; Zheng, Y.; Yan, H.; Facchetti, A. *J. Am. Chem. Soc.* **2009**, *131*, 8−9.

(24) Yan, H.; Chen, Z.; Zheng, Y.; Newman, C.; Quinn, J. R.; Dötz, F.; Kastler, M.; Facchetti, A. *Nature* **2009**, *457*, 679−686.

(25) Baeg, K.; Khim, D.; Jung, S.; Kang, M.; You, I.; Kim, D.; Facchetti, A.; Noh, Y. *Adv. Mater.* **2012**, *24*, 5433−5439.

(26) Gao, X.; Di, C.; Hu, Y.; Yang, X.; Fan, H.; Zhang, F.; Liu, Y.; Li, H.; Zhu, D. *J. Am. Chem. Soc.* **2010**, *132*, 3697−3699.

(27) Zhao, Y.; Di, C.; Gao, X.; Hu, Y.; Zhang, L.; Liu, Y.; Wang, J.; Hu, W.; Zhu, D. *Adv. Mater.* **2011**, *23*, 2448−2453.

(28) Hu, Y.; Gao, X.; Di, C.; Yang, X.; Zhang, F.; Liu, Y.; Li, H.; Zhu, D. *Chem. Mater.* **2011**, *23*, 1204−1215.

(29) Suraru, S. L.; Zschieschang, U.; Klauk, H.; Würthner, F. *Chem. Commun.* **2011**, *47*, 11504−11506.

(30) (a) Tan, L.; Guo, Y.; Zhang, G.; Yang, Y.; Zhang, D.; Yu, G.; Xu, W.; Liu, Y. *J. Mater. Chem.* **2011**, *21*, 18042−18048. (b) Tan, L.; Guo, Y.; Yang, Y.; Zhang, G.; Zhang, D.; Yu, G.; Xu, W.; Liu, Y. *Chem. Sci.* **2012**, *3*, 2530−2541.

(31) (a) Herbst, M.; Hunger, K. *Industrial Organic Pigments*; VCH: New York, 1993. (b) Herbst, W.; Hunger, K. *Industrial Organic Pigments, Production, Properties, Applications*; Wiley-VCH: Weinheim, 1997.

(32) Quinto, M.; Jenekhe, S. A.; Bard, A. J. *Chem. Mater.* **2001**, *13*, 2825−2834.

(33) Babel, A.; Jenekhe, S. A. *J. Am. Chem. Soc.* **2003**, *125*, 13656−13657.

(34) Langhals, H.; Jaschke, H. *Chem.—Eur. J.* **2006**, *12*, 2815−2824.

(35) Ortiz, R. P.; Herrera, H.; Seoane, C.; Segura, J. L.; Facchetti, A.; Marks, T. J. *Chem.—Eur. J.* **2012**, *18*, 532−536.

(36) Polander, L. E.; Pandey, L.; Romanov, A.; Fonari, A.; Barlow, S.; Seifried, B. M.; Timofeeva, T. V.; Brédas, J.; Marder, S. R. *J. Org. Chem.* **2012**, *77*, 5544−5551.

(37) Durban, M. M.; Kazarinoff, P. D.; Segawa, Y.; Luscombe, C. K. *Macromolecules* **2011**, *44*, 4721−4728.

(38) (a) Chopin, S.; Chaignon, F.; Blart, E.; Odobel, F. *J. Mater. Chem.* **2007**, *17*, 4139−4146. (b) Würthner, F.; Suraru, S.-L. *Synthesis* **2009**, *2009*, 1841−1845.
(39) (a) Kondo, M.; Uchikawa, M.; Namiki, K.; Zhang, W.; Kume, S.; Nishibori, E.; Suwa, H.; Aoyagi, S.; Sakata, M.; Murata, M.; Kobayashi, Y.; Nishihara, H. *J. Am. Chem. Soc.* **2009**, *131*, 12112−12124. (b) Kondo, M.; Uchikawa, M.; Kume, S.; Nishihara, H. *Chem. Commun.* **2009**, *45*, 1993−1995.
(40) Rao, K.; Kusamoto, T.; Toshimitsu, F.; Inayoshi, K.; Kume, S.; Sakamoto, R.; Nishihara, H. *J. Am. Chem. Soc.* **2010**, *132*, 12472−12479.
(41) Kondo, M.; Uchikawa, M.; Zhang, W.; Namiki, K.; Kume, S.; Murata, M.; Kobayashi, Y.; Nishihara, H. *Angew. Chem., Int. Ed.* **2007**, *46*, 6271−6274.
(42) Compound **1g** shows almost the same absorption spectra (see Figure S1, Supporting Information) as **1a**. This is understandable as they contain the same conjugated moieties.
(43) As an example, the absorption spectrum of **1b** was measured in solvents of different polarities (see Figure S3, Supporting Information). The absorption spectrum of **1b** was slightly red-shifted in polar solvents. Moreover, the fluorescence spectrum of **1b** was largely red-shifted in acetone and ethyl acetate compared to that in hexane. These results provide the support for existence of intramolecular interactions between the respective electron-donating and -accepting moieties in **1a**−**d**.
(44) As an example, the femtosecond transient absorption spectra of **1b** in benzonitrile were measured after irradiation. Figures S6−S8 (Supporting Information) show the absorption spectra at different delay times, the time profile of the transient absorption at 540 nm, and the time profile of the transient absorption at 650 nm. According to previous reports, the absorption at 650 nm should be due to the radical cation of triphenylamin: Oyama, M.; Nozaki, K.; Okasaki, S. *Anal. Chem.* **1991**, *63*, 1387−1392. De la Fuente, J.; Neira, V.; Saitz, C.; Jullian, C.; Sobarzo-Sanchez, E. *J. Phys. Chem. A* **2005**, *109*, 5897−5904. Therefore, the formation of the radical cation of triphenylamine upon photoirradiation provides direct evidence for the photoinduced electron transfer between the triphenylamine moieties and the central core in **1b** upon light irradiation. In addition, the free-rotation of phenyl fragments within triphenylamine moieties will also lead to weak fluorescence of **1b** in solution.
(45) This can be again attributed to the intramolecular photoinduced electron transfer between ferrocene moieties and the electron-accepting central conjugated core.
(46) (a) Kuwabara, J.; Yamagata, T.; Kanbara, T. *Tetrahedron* **2010**, *66*, 3736−3741. (b) Mei, J.; Wang, J.; Sun, J.; Zhao, H.; Yuan, W.; Deng, C.; Chen, S.; Sung, H. H. Y.; Lu, P.; Qin, A.; Kwok, H.; Ma, Y.; Williams, I. D.; Tang, B. *Chem. Sci* **2012**, *3*, 549−558.
(47) Lei, T.; Chen, H.; Yin, J.; Huang, S.; Zhu, X.; Pei, J. *Org. Electron.* **2011**, *12*, 453−460.
(48) Both photoinduced electron-transfer and free rotations of phenyl fragments within triphenylamine moieties contribute to the weak fluorescence of **1b** in solution. In the solid state, **1b** may adopt a more twisting conformation, and as a result the intramolecular electron donor−acceptor interactions may be weakened; accordingly, the photoinduced electron transfer may become less effective in comparison with that in solution. More importantly, the free rotations can be inhibited in the solid state (after aggregation). These synergic effects may lead to fluorescent enhancement for **1b** in the solid state (after aggregation).
(49) Dong, Y.; Lam, J. W. Y.; Qin, A.; Li, Z.; Sun, J.; Sung, H. H.-Y; Williams, I. D.; Tang, B. *Chem. Commun.* **2007**, *43*, 40−42.
(50) Hong, Y.; Lam, J. W. Y.; Tang, B. *Chem. Soc. Rev.* **2011**, *40*, 5361−5388.
(51) Qi, X.; Li, H.; Lam, J. W. Y.; Yuan, X.; Wei, J.; Tang, B.; Zhang, H. *Adv. Mater.* **2012**, *24*, 4191−4195.
(52) Zeng, Q.; Li, Z.; Dong, Y.; Di, C.; Qin, A.; Hong, Y.; Ji, L.; Zhu, Z.; Jim, C. K. W.; Yu, G.; Li, Q.; Li, Z.; Liu, Y.; Qin, J.; Tang, B. *Chem. Commun.* **2007**, *43*, 70−78.
(53) Deans, R.; Kim, J.; Machacek, M. R.; Swager, T. M. *J. Am. Chem. Soc.* **2000**, *122*, 8565−8566.
(54) Efforts were made to prepare the single crystals of **1b** to determine the structure of **1b** in the solid state, but failed.
(55) (a) Wu, Y.; Li, J.; Ai, X.; Fu, L.; Zhang, J.; Fu, Y.; Zhou, J.; Li, L.; Bo, Z. *J. Phys. Chem. A* **2007**, *111*, 11473−11479. (b) Liu, H.; Jia, H.; Wang, L.; Wu, Y.; Zhan, C.; Fu, H.; Yao, J. *Phys. Chem. Chem. Phys.* **2012**, *14*, 14262−14269.
(56) Compared to the oxidation potentials of free ferrocene and triphenylamine (see Figure S10, Supporting Information), the oxidation potentials of **1a** and **1b** were positively shifted by 0.10 and 0.04 V, respectively. This is probably due to the respective intramolecular electron donor−acceptor interactions within **1a** and **1b**.
(57) De Leeuw, D. M.; Simenon, M. M. J.; Brown, A. R.; Einerhand, R. E. F. *Synth. Met.* **1997**, *87*, 53−59.
(58) Usta, H.; Facchetti, A.; Marks, T. J. *J. Am. Chem. Soc.* **2008**, *130*, 8580−8581.
(59) Because of the limitation of calculation capacity, the DFT calculations were not performed for **1a** and **1b**.
(60) The differences may result from the fact that the solvent effects were not included in the calculations.
(61) However, domain sizes decrease after further annealing at 120 °C. Also, XRD diffraction peaks become weak. These are in agreement with the observation that hole mobility of OFETs of **1c** decreases after further annealing at 120 °C (see Table S1, Supporting Information).
(62) Meng, H.; Bao, Z.; Lovinger, A. J.; Wang, B. C.; Mujsce, A. M. *J. Am. Chem. Soc.* **2001**, *123*, 9214−9215.
(63) Wu, Y.; Li, Y.; Gardner, S.; Ong, B. S. *J. Am. Chem. Soc.* **2005**, *127*, 614−618.
(64) The existence of contact resistance is probably due to the fact that the HOMO level of **1c** (−5.76 eV) does not match the work function of gold electrodes, and thus, the injection barrier is induced.
(65) Chaignon, F.; Falkenström, M.; Karlsson, S.; Blart, E.; Odobel, F.; Hammarström, L. *Chem. Commun.* **2007**, *43*, 64−66.
(66) Dallairel, C.; Brook, M. A. *Organometallics* **1993**, *12*, 2332−2338.